Materials Science in Semiconductor Processing 195 (2025) 109617

Contents lists available at ScienceDirect

Materials Science in Semiconductor Processing

journal homepage: www.elsevier.com/locate/mssp

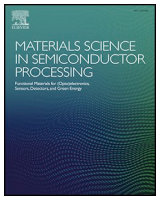

Optical properties of carbon nitride thin films fabricated by rapid chemical vapor deposition

Eugene Chubenko *, Sergey Maximov, Cong Doan Bui, Victor Borisenko

Belarusian State University of Informatics and Radioelectronics, P. Browka Str. 6, Minsk, 220013, Belarus

ARTICLE INFO

Keywords:
Carbon nitride
Optical spectroscopy
Thin film
Swanepoel's envelope method
Refractive index
Extinction coefficient

ABSTRACT

Developed rapid chemical vapor deposition lasting only 3 min allowed to produce smooth layered carbon nitride polycrystalline thin films as thick as 830–1547 nm at 550–625 °C in air with crystallites in the layers oriented parallel to the substrate (glass or silicon) surface. They are distinguished by high transparency in the visible range and the thickness uniformity. It made possible an adequate optical transmission and absorption spectra measurements at room temperature and their correct processing with the Swanepoel's envelope method to determine optical properties of the films and compare them with characteristics of carbon nitride materials obtained by conventional chemical vapor deposition or thermal polymerization. The application of the Swanepoel's method allowed to determine actual thickness of the films and then the refraction index of the material to be 2.50–3.25 and the extinction coefficient to be 0.1–0.4 as functions of the deposition temperature. The average photoluminescence lifetime of the deposited material is found to be 2.3–2.6 ns for high energy carrier recombination processes being the shortest in the sample fabricated at 550 °C and correlating with crystallinity of the film. Optimal temperature for rapid chemical vapor deposition of carbon nitride thin films is concluded to be in the range of 550–575 °C providing its best properties promising for electronic and optoelectronic applications.

1. Introduction

The Noble-prize-winning experiments with graphene [1] has sparked an interest to 2D materials. Their layered structure demonstrates electronic and optical properties varied between bulk and atomic monolayer forms. More crucially, they may be altered for certain applications being dependent on the thickness or, more precisely, the number of layers constituting the thin film [2]. With certain exceptional benefits including stability, affordability, and earth-abundance, so-called graphitic carbon nitride is a 2D material which has received a lot of interest and attention especially in photochemistry, energy conversion, and storage applications [3]. It has structural similarities to multilayered graphene and the band gap of about 2.7 eV at room temperature [4], which is significant for UV and visible range photocatalysis and optoelectronics. Commonly named as "graphitic carbon nitride" this material usually consists of polymeric chains of stacked heptazine units and more accurately should be addressed as "polymeric carbon nitride" (pCN) [5–7], as we do in this article.

Nitrogen rich organic precursors are used for pCN synthesis. Melamine, urea, cyanamide, dicyandiamide, and benzoguanamine are the most common one [4,8]. Due to its availability and low cost, direct thermal polycondensation (calcination) they are often used for synthesis of pCN [8]. Basically, the precursor is heated for several hours at a temperature between 300 and 700 °C in a controlled atmosphere or under vacuum to produce bulk pCN. It can be then grinded down or exfoliated by ultrasonic, chemical or mechanical methods. The resulted powder and particles are mostly suitable only for photocatalytic applications [8–10]. However, uniform pCN thin films or 2D structures are of greater interest for optoelectronic and electronic devices [11]. This is necessary for effective charge transfer from the thin film to the substrate or to put it another way to improve the thin film performance, in particular applications in photocatalysis, photovoltaics and electronics [7,8]. It was already shown by several research groups that desired objects could be fabricated by variety of chemical vapor deposition (CVD) methods [7,11–18]. They are usually being implemented in a tube two-zone reactor with a separated space between the precursor and substrates. The deposition cycle lasts for hours with rather slow heating rate in the range of 5–20 °C/min. Rapid CVD of pCN with an overall processing time decreased to 3–10 min was also demonstrated [19].

In contrast to thoroughly studied photocatalytic properties of pCN its

* Corresponding author.
E-mail address: eugene.chubenko@gmail.com (E. Chubenko).

https://doi.org/10.1016/j.mssp.2025.109617
Received 18 February 2025; Received in revised form 1 April 2025; Accepted 25 April 2025
Available online 2 May 2025

optical properties in particular in the form of 2D layered films remain less known [7]. Meanwhile, they are important for most optical and optoelectronic applications. Recently, pCN thin films were observed to possess the refractive index of 2.3–2.5 in the visible range [7], which is among the highest ones recorded for polymeric materials. Thus, an extended study of optical properties of 2D pCN layered films looks indeed promising.

In this paper we present optical characteristics of pCN thin films deposited on silicon and glass substrates by rapid CVD at different temperatures and compare them with those of the material fabricated in a conventional "slow" CVD [7,11–18]. They are also extended by the photoluminescence (PL) dynamics data with their extracted PL lifetime parameters.

2. Experimental

The pCN thin film was deposited by the rapid CVD [19] on 1 mm thick the 1 × 3 inch rectangular glass substrates (ApexLab, China) and 3-inch monocrystalline p-type silicon wafers covered by 290 nm silicon oxide (SiO_2) layer. Glass funnel with 4 mm thick porous membrane at the bottom was used for that (Fig. 1). Porous membrane was made of sintered glass particles. Diameter of the pores in the membrane was around 100 μm. Powdered melamine (Sigma-Aldrich) with the purity of 99 % was placed inside the funnel on the porous surface. A preliminary acetone cleaned substrate (silicon or glass) was then put on the top of the funnel. Funnel with the substrate was placed inside the air-filled Nabertherm 9L/330 muffle furnace already heated to a target temperature in the range of 550–625 °C. After exposing the whole set at this temperature for 3 or 5 min the substrate was rapidly extracted from the furnace and cooled down to room temperature in air.

The film morphology was analyzed with SEM using Hitachi S-4800. The atomic composition of the films was examined with Bruker QUANTAX 200 EDX spectrometer. Surface images and topological microprofiles were obtained using AFM Microtestmachines NT-206. Crystalline phases in the films were identified by XRD analysis using DRON-4 diffractometer equipped with Cu Kα source ($\lambda = 1.5406$ Å).

A Proscan MC121 spectrophotometer was used to examine the optical transmission and reflection spectra of the samples at room temperature in the wave range of 350–900 nm. In order to calculate the refractive index, extinction coefficient and thickness of thin films from the absorption/transmission spectra we used Swanepoel's envelope method [20,21].

Photoluminescence spectra were recorded at room temperature with SOLAR TII MS7504i spectrophotometer equipped with Proscan HS101 CCD camera as a detector. PL excitation was implemented by 345 nm (3.59 eV) monochromatic line from 1 kW Xe lamp cut out from its total spectrum by SOLAR TII DM 160 double monochromator. The PL decay kinetics measurements were carried out using a 375 nm laser LED operating at pulsed mode with pulse duration of 800 ns and a Hamamatsu C4334 streak camera with a temporal resolution of 20 ps and spectral resolution of 1 nm.

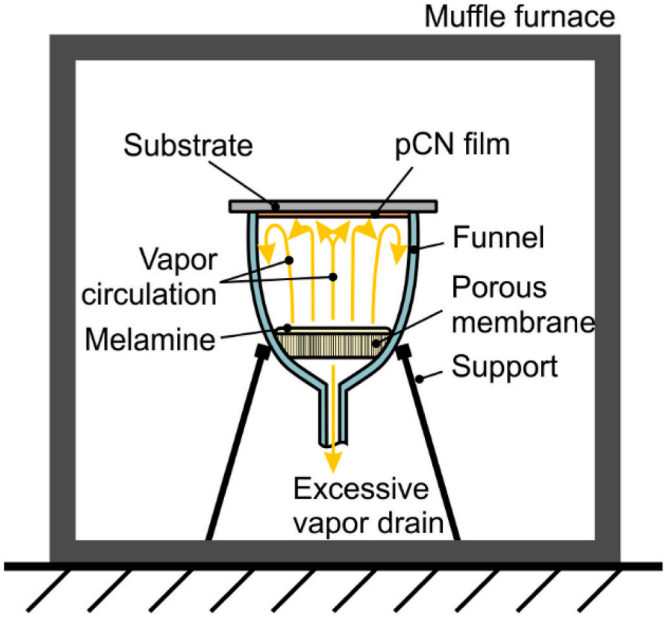

Fig. 1. Schematic illustration of the pCN film deposition process.

3. Results

3.1. Structure and composition

The scanning electron microscopy (SEM) analysis performed showed the films deposited on the both silicon and glass substrates to have smooth surface and layered structure (Fig. 2, a). Air/film and film/substrate interfaces are parallel to each other. According to atomic force microscopy (AFM) study the surface roughness of the films is less than 4–6 nm for each sample (Fig. 2, b). The thickness of the films is a convex function of the deposition temperature with an extremum at around 600 °C (Fig. 3, a). According to data extracted from SEM images an increase of the temperature to this point leads the thickness of the films to increase from 860 nm at 550 °C to 1540 nm and then to decrease back to 873 nm at 625 °C (see also Table 1).

Energy-dispersive X-ray (EDX) spectroscopy results have confirmed that the deposited films consist of carbon and nitrogen with a certain amount of oxygen. Carbon/nitrogen atomic concentration ratio C_C/C_N

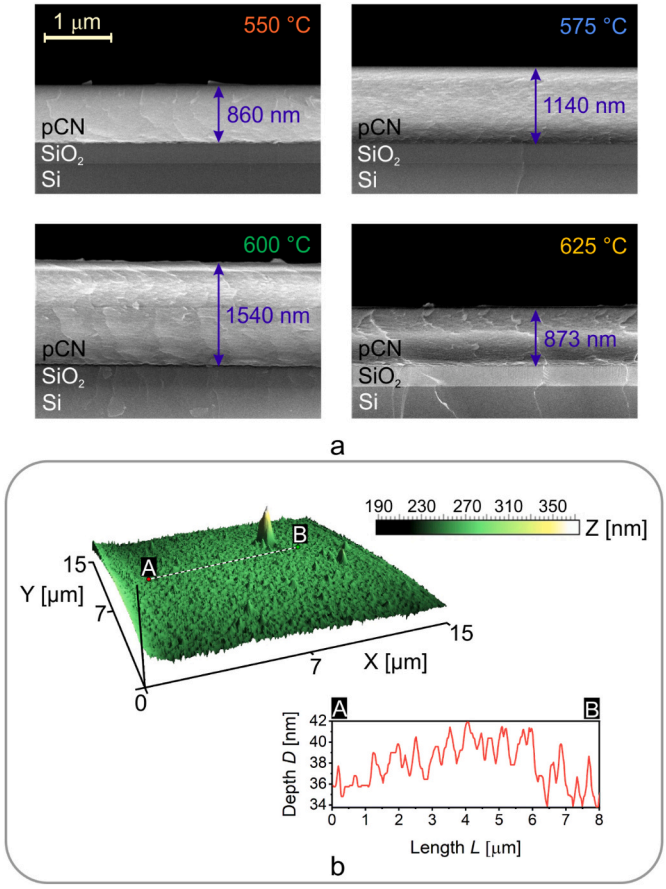

Fig. 2. Cross-section SEM images of the films deposited on silicon substrate with SiO_2 sublayer at different temperatures (a), typical AFM image and depth profile of the film surface (b).

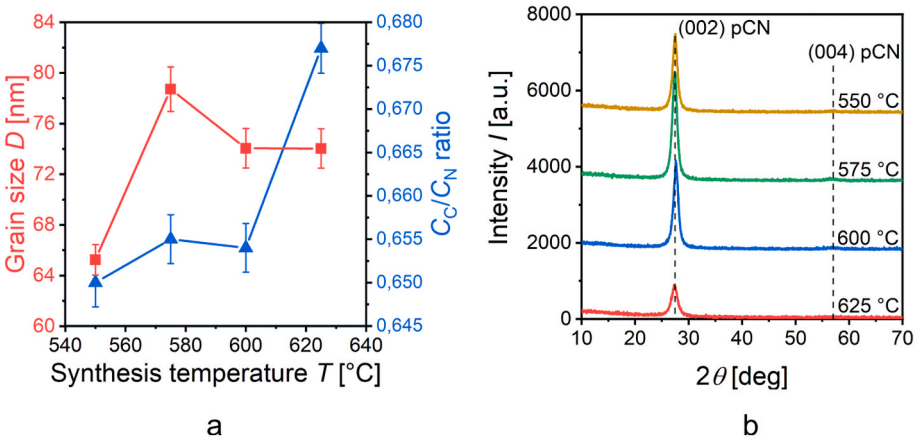

Fig. 3. Carbon (C_C) and nitrogen (C_N) atoms concentration ratio and grain size *vs.* deposition temperature plot (a) and XRD plot (b) of the samples fabricated at different temperatures.

Table 1
Thickness of the pCN thin films deposited at different temperatures and process durations on glass substrates determined using different methods.

Deposition temperature T [°C]	Process duration t [min]	Thickness of the films d [nm]		
		Derived from SEM images	Calculated using Swanepoel's method	Difference [%]
550	3	860	654	24.0
575	3	1140	1167	2.0
600	3	1540	1547	0.5
625	3	873	765	12.0
625	5	950	830	13.0

increases gradually with the temperature from 0.65 to 0.68 (blue line in Fig. 3, a). These are close to the stoichiometric ratio of 0.75 for fully polymerized graphitic carbon nitride [5]. The oxygen content is close but do not exceed 2.9 at.% in all samples.

X-ray diffraction (XRD) patterns (Fig. 3, b) show the prominent peak around $2\theta = 27.5$ deg associated with the reflex from pCN (002) hexagonal crystal plane and weak peak around $2\theta = 56.5$ deg corresponding to reflection from the (004) plane [8]. The peak corresponding to the (210) plane located around $2\theta = 12$–13 deg and usually presented on XRD spectra of bulk or powdered pCN is not seen on the graphs presented in Fig. 3, b. It means, that the fabricated films are strongly oriented, and their (002) crystal plane are parallel to the substrate surface. The intensity of the pCN (002) XRD reflexes reaches its maximum at the deposition temperature of 600 °C. That follows the thickness *vs.* synthesis temperature relations.

The size of crystallites in the films D calculated according the Scherrer equation is also a convex function of the deposition temperature increasing from 65 nm upon processing at 550 °C to 78 nm for the film deposited at 575 °C. With a further increase of the temperature, the crystallite size decreases to ~74 nm (Fig. 3, a). The interplane distance decreased from 3.25 to 3.22 Å with the temperature growing from 550 to 575 °C and then increases up to about 3.24 at 600–625 °C.

According to the results presented the deposited films could be considered as layered well-structured polycrystalline carbon nitride.

3.2. Absorption, refractive index and extinction coefficient

Considering the SEM results light propagation across the pCN thin films deposited on glass substrate could be schematically represented as illustrated in Fig. 4. Here we assume that the light comes perpendicular to the surface of the substrate, and that the substrate itself is thick, finite, and transparent. We also assume that the sample is in an air

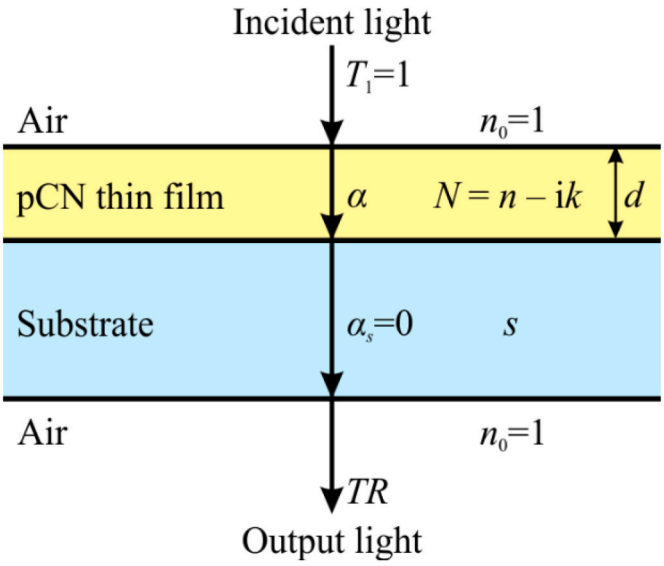

Fig. 4. Schematic of light propagation across an absorbing thin film on a thick finite transparent substrate.

environment, the refractive index of which is $n_0 = 1$. The incident light intensity is $T_1 = 1$ a.u. Complex refractive index N of pCN could be defined as $N = n - ik$, where n is the real part of the complex refractive index (phase velocity) and k is the extinction coefficient. The last is related to the absorption coefficient of the pCN film α by the equation $k = \alpha\lambda/4\pi$. The thickness of pCN film is d.

The glass substrate refractive index s could be determined using its optical transmission spectrum. It was found to be $s = 1.595$ for the glass substrates used in our experiments. It is implied to be almost independent on the wavelength of the incident light. We also suppose that the substrate is ideally transparent compared to the deposited film and its absorption coefficient $\alpha_s = 0$.

In that case the transmittance TR as a function of the film thickness d and light wavelength λ variables $x = e^{-\alpha d}$ and $\varphi = 4\pi nd/\lambda$ [21,22]:

$$TR = \frac{Ax}{B - Cx\cos(\varphi) + Dx^2}, \quad (1)$$

where the coefficients could be expressed as:

$A = 16n^2 s$;

$$B = (n+1)^3(n+s^2);$$

$$C = 2(n^2-1)(n^2-s^2);$$

$$D = (n-1)^3(n-s^2).$$

Experimental transmission and absorption spectra of pCN films deposited on the glass substrate are shown in Fig. 5.

The transmittance of pCN films becomes 20 % increased upon the deposition temperature was increased from 550 to 600 °C. There is no much difference in the curves corresponding to the samples fabricated at the same temperature and different deposition process times altered from 3 to 5 min. For the sample with the longer deposition time the transmission is a little bit higher.

Two wavelength-dependent envelope curves were constructed according the Swanepoel's method on the basis of the above transmission spectra [21,22]. The first is a tangent to the minima $T_m(\lambda)$ of the interference fringes and corresponds to $\cos(\varphi) = -1$ in Eq. (1). The second envelope curve $T_M(\lambda)$ is a tangent to the maxima of the interference fringes and could be described by Eq. (1) with $\cos(\varphi) = 1$. Using derived $T_m(\lambda)$ and $T_M(\lambda)$ functions we could calculate the real part of the refractive index by the equation:

$$n = \left[N_1^2 + (N_1^2 - s^2)^{\frac{1}{2}}\right]^{\frac{1}{2}}, \quad (2)$$

where

$$N_1 = \frac{2s}{T_m(\lambda)} + \frac{s^2+1}{2}$$

for transparent region and

$$N_1 = 2s\frac{T_M(\lambda) - T_m(\lambda)}{T_M(\lambda)T_m(\lambda)} + \frac{s^2+1}{2}$$

for the weak and medium absorption regions. It should be noted, that using this method the refractive index could only be determined in low and medium absorption spectral ranges.

The neighboring interference fringes located at the wavelengths λ_1 and λ_2 were used to calculate the thickness of the films using the relationship [22]:

$$d = \frac{\lambda_1\lambda_2}{2(n_{\lambda 2}\lambda_1 - n_{\lambda 1}\lambda_2)}. \quad (3)$$

Values of the refractive indexes $n_{\lambda 1}$ and $n_{\lambda 2}$ corresponding to the wavelengths λ_1 and λ_2 are taken from the data calculated by Eq. (2).

Note that smooth envelope curves are often difficult to generate properly [22,23]. Accumulated minor errors lead to incorrect determination of refractive index and thickness. The correction algorithm should be used to obtain more real values. On the first step average film thickness should be calculated d_{average} using a set of values derived for each sample with Eq. (3). Using the averages thickness and refractive index corresponding to the wavelength positions of the interference minimum and maximum the order number m of the interference extrema could be determined as:

$$2nd = m\lambda. \quad (4)$$

Then the obtained order numbers should be rounded off to the nearby integer (for interference maxima) or half-integer (for minima) and accepted as an exact order number m_{corr} for each extremum. Thus, more accurate corrected film thickness d_{corr} can be derived using Eq. (4) and accepted values of m_{corr}. The values of d_{corr} calculated for each interference minimum and maximum have the smallest dispersion. It allows to get more accurate film thickness values by averaging the set of d_{corr}. Obtained average film thickness of our samples are presented in Table 1 in comparison with the data extracted from SEM images (see. Fig. 2, a).

Using Eq. (4) and average values of d_{corr} for each sample more accurate values of refractive index were obtained. They are presented in Fig. 6, a by scattered symbols. Due to the low signals in the high absorbance range the refractive index could not be defined there. In order to overwhelm that, it is preferred to extrapolate the refractive index experimental data using Cauchy equation [22–26]. Frequently only two or three-terms Cauchy equation are used:

$$n(\lambda) = a + b/\lambda^2 + c/\lambda^4. \quad (5)$$

Here a, b and c are empirical fitting parameters. Also, the wavelength has to be expressed in microns. The extrapolation curves constructed using Eq. (5) are presented in Fig. 6, a. The derived refractive index n in the visible range varies as a function of the film deposition temperature between 2.50 and 3.25. Obtained values are higher than refractive index of the pCN films fabricated by "slow" thermochemical vapor deposition process described elsewhere [7].

The extinction coefficient $k(\lambda)$ was calculated through absorbance coefficient $\alpha(\lambda)$ which was determined using absorbance $Abs(\lambda)$ and corrected film thickness d_{corr} derived by the Swanepoel's method (Fig. 6, b).

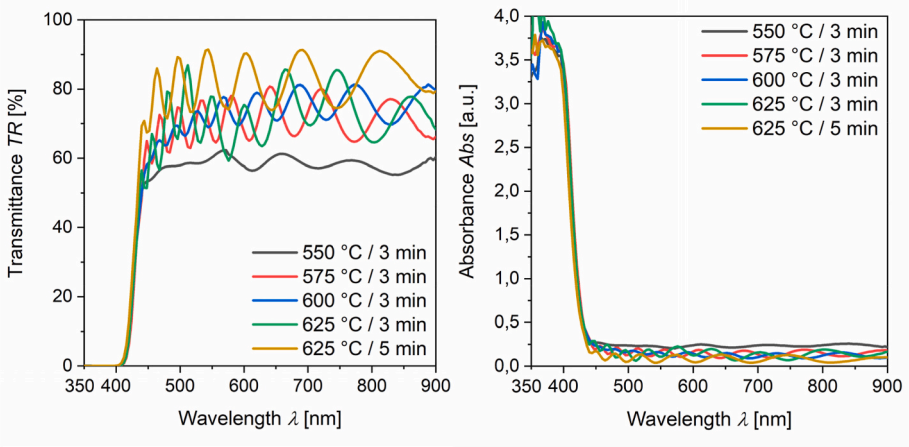

a b

Fig. 5. Transmission (a) and absorption (b) spectra of pCN thin films deposited on glass substrates at different temperatures and process durations. The absorption was calculated as $Abs = -2.3026 \cdot \log(TR)$.

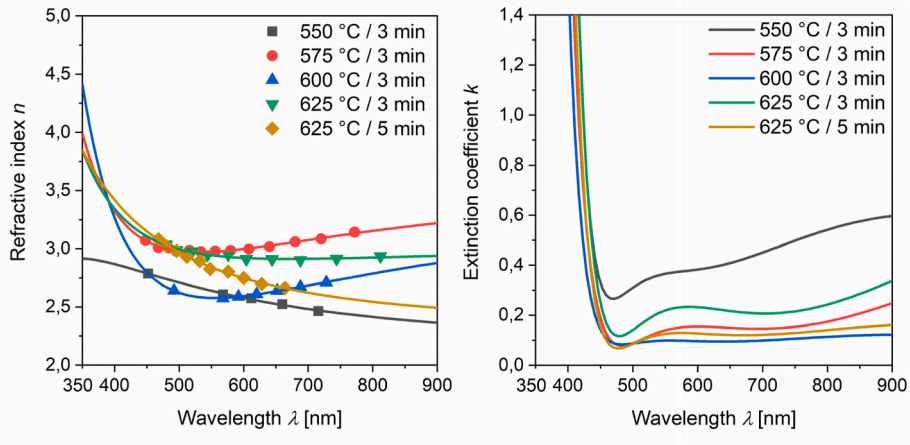

a b

Fig. 6. Refractive index (a) and extinction coefficient (b) of thin film pCN deposited on glass substrates at different temperatures and process durations.

3.3. Optical band gap

The optical band gap of the deposited pCN was evaluated from the absorbance spectra reconstructed to the Tauc plot coordinates, as it is shown in Fig. 7. The tangent lines of the absorbance allow determination of values of direct and indirect band gaps of the material. The values obtained are presented in Table 2.

The direct band gap slightly varies between 2.96 and 2.99 eV across the whole temperature range used for the synthesis of pCN. But it has a tendency to decrease with the growing temperature. The process duration increase leads to a wider band gap (3.00 eV). Meanwhile, the indirect band gap remains practically invariable being 2.79–2.80 eV.

Table 2
Optical band gaps of the thin film pCN deposited at different temperatures and process duration on glass substrates determined using Tauc plots.

Deposition temperature T [°C]	Process duration t [min]	Band gap E_g [eV]	
		direct	indirect
550	3	2.99	2.80
575	3	2.96	2.79
600	3	2.97	2.79
625	3	2.96	2.80
625	5	3.00	2.80

3.4. Photoluminescence

PL spectra of the fabricated pCN thin films are illustrated in Fig. 8. The position of the PL intensity peak slightly shifts to longer wavelengths (from 473 to 476 nm) with an increase of the deposition temperature. As the deposition temperature grows up the top parts of the PL bands become broaden, the peaks themselves appear to be less prominent, and overall PL intensity decreases. The full width on half maximum (FWHM) of the PL spectra increases with temperature from 101 nm for the film deposited at 550 °C to 111 nm for the sample obtained at 625 °C (see inset on Fig. 8).

To obtain PL decay curves the several wavelengths were chosen on recorded PL spectra. They are indicated in Fig. 8. Selected wavelengths are distributed along the observed PL band and approximately correspond to the energy of radiative recombination processes identified in pCN materials [26,27]. Obtained normalized PL decay curves of pCN films synthesized at 550 and 625 °C are presented in Fig. 9. The decay curves $I(t)$ are strongly nonexponential, indicating a broad distribution of lifetimes of the excited electronic states. As the detection wavelength grows the PL decay also gradually increases.

The decay of the PL intensity $I(t)$ was fitted with the triexponential

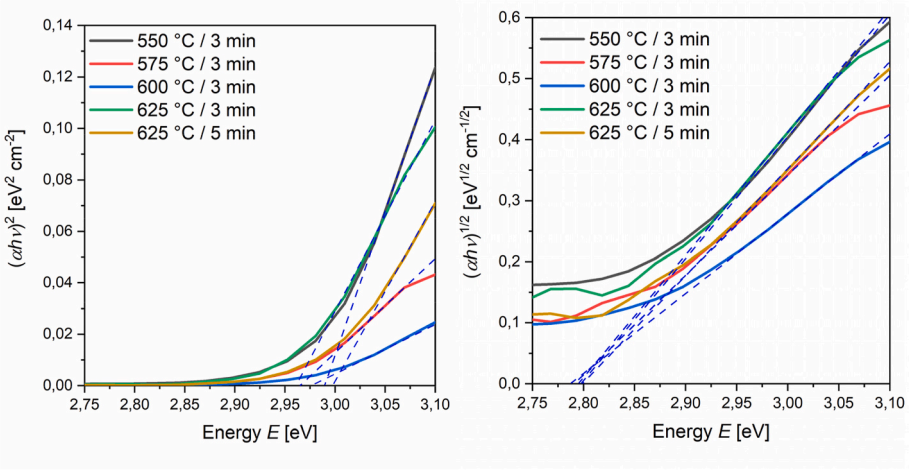

a b

Fig. 7. Tauc plots for direct (a) and indirect (b) band gaps of thin film pCN deposited on glass substrates at different temperatures and process durations.

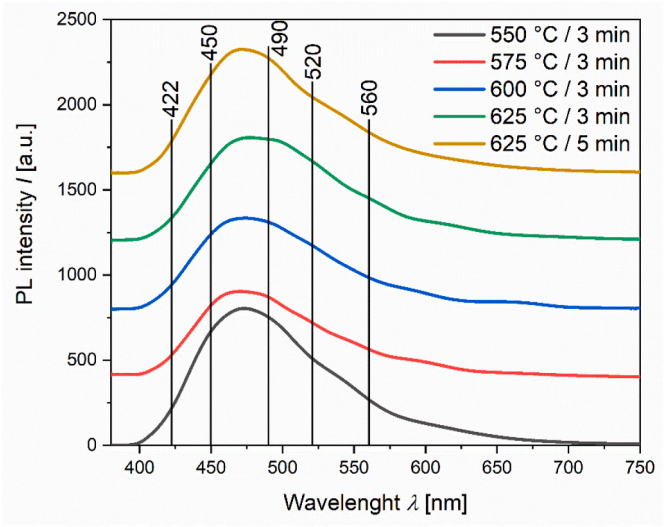

Fig. 8. Room temperature PL spectra of the pCN films deposited on silicon substrates at different temperatures and process durations.

equation using DAS6 (HORIBA Scientific) software:

$$I(t) = A + B_1 e^{-t/\tau_1} + B_2 e^{-t/\tau_2} + B_3 e^{-t/\tau_3} \quad (6)$$

Here A is a time independent constant, B_n are relative amplitudes of the PL processes with the lifetimes of τ_n. Each component of Eq. (6) could be associated with different radiative recombination processes in pCN which include electron transitions between oxygen and nitrogen defects related energy levels, conductance and valence bands [26,27].

The above fitting parameters as a function of the detection wavelengths are presented in Fig. 10. The lifetime of each process increases with the registration wavelength. For the pCN film deposited at 550 °C compared to the sample fabricated at 625 °C the lifetimes are longer in the detection wavelength range studied. The lifetimes τ_1 and τ_2 corresponding to the first two components of Eq. (6) are relatively short and do not exceed 10 ns. The amplitudes B_1 and B_2 of these components decrease with an increase of the detection wavelength but they remain bigger than that of the third component.

The third "slow" component is characterized by much longer lifetime with more prominent dependence on the detection wavelength. Its lifetime τ_3 increases from 10 ns up to 42–56 ns with the detection wavelength. At the same time relative amplitude B_3 is almost doubled at the detection wavelength of 560 nm and becomes very close to B_2.

The average lifetime τ_{av} was calculated as:

$$\tau_{av} = \frac{B_1\tau_1^2 + B_2\tau_2^2 + B_3\tau_3^2}{B_1\tau_1 + B_2\tau_2 + B_3\tau_3}. \quad (7)$$

Fig. 10 shows that the calculated τ_{av} value also increases with the detection wavelength from 2.6 to 17.5 ns for the pCN film fabricated at 550 °C and from 2.3 to 14.3 ns for the sample processed at 625 °C.

4. Discussion

The deposited thin films were observed to be polycrystalline, well-structured with the crystalline grains oriented along the surface of the substrate used. The strong peak on XRD plots (Fig. 3, b) corresponding to X-ray reflection from hexagonal (002) planes of g-C_3N_4 and an absence of (210) peak associated with their in-plane scattering from heptazine-like building units confirm good crystallization of the deposited material [8,28]. While the composition of the films is substoichiometric, as C_C/C_N ratio remains below 0.75 evident for stoichiometric C_3N_4, the interplane distance between the layers is under 3.26 Å – the value inherent to the completely polymerized material [28]. Compression of the crystal lattice is presumably a result of the observed stoichiometry violation and oxygen content.

Size variation of the crystallites as a function of the deposition temperature (Fig. 3, a) and evolution of the interplane distance indicate that the best crystallinity is achieved upon deposition at around 575 °C. At higher temperatures the crystallites appear to be smaller while interplane distance grows up. It could be a result of partial decomposition and/or evaporation of the material just synthesized at the substrate. Note, that decomposition looks to be less possible to play a main role because the C_C/C_N ratio increases with the deposition temperature reflecting the reduction of excess of nitrogen atoms. The bonds between heptazine molecules in the melon polymer chains or graphitic carbon nitride sheets are formed by the three –NH_2 amino groups located around heptazine molecule core formed by three aromatic rings with an alternating arrangement of carbon and nitrogen atoms [5,7]. The formation of bonds between two heptazine molecules accompanied by the loss of one nitrogen atom as a part of ammonia NH_3 and the formation of –NH– bridge between them. Hence the growth of C_C/C_N ratio indicates the increase of polymerization rates as more heptazine molecules are combined with each other [5]. Decomposition of the formed pCN material usually followed by the decrease in the C_C/C_N ratio [8,9,18,29] is unlikely in this case. Hence the reduction of the film thickness upon deposition at above 600 °C (see Table 1) may be caused by congruent

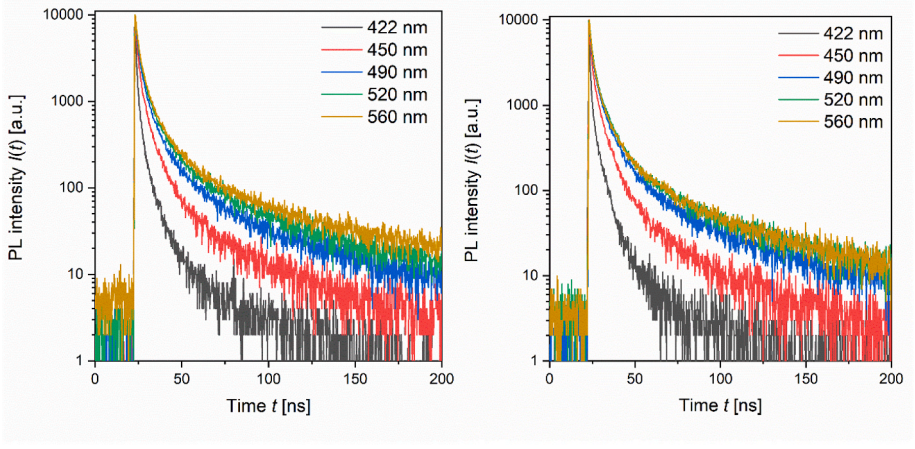

Fig. 9. Normalized room temperature PL decay curves of pCN thin films deposited on silicon substrates at 550 (a) and 625 °C (b) recorded at different detection wavelengths.

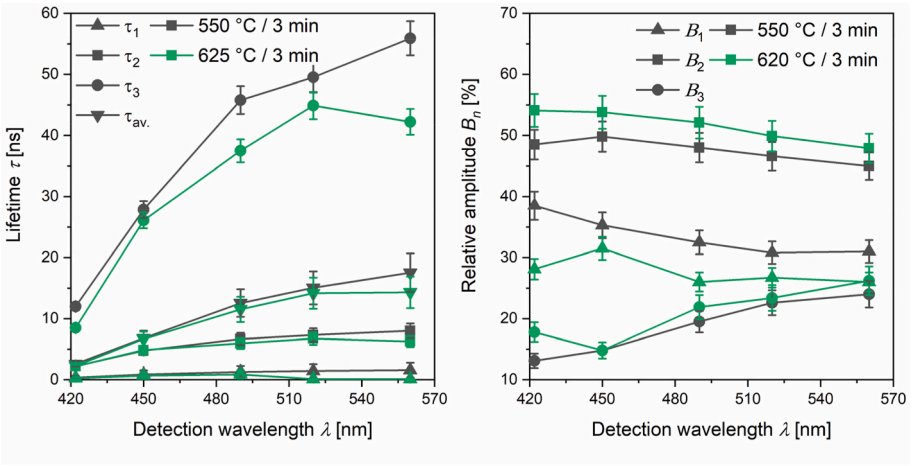

Fig. 10. Room temperature PL lifetimes (a) and corresponding relative amplitudes of each PL process (b) for pCN thin films synthesized at 550 and 625 °C on silicon substrates.

sublimation as far as no surface cracks and voids were observed on SEM images (Fig. 2, a).

Smooth surface and high transparency of the films provided their correct spectroscopic analysis in the optical range and thickness determination. For the middle of the temperature range used for pCN deposition (575–600 °C) the thickness of the films derived using Swanepoel's method are close to the values directly extracted from SEM images (the difference is 0,5–2 %, see Table 1). It indicates the good construction of $T_m(\lambda)$ and $T_M(\lambda)$ envelope curves. However, for the highest and lowest deposition temperatures of 550 and 625 °C obtained thickness difference reaches 12–24 %. The reason for this is the insufficient number of extreme points, the number of which decreases in the limited transmittance measurement spectral range with decreasing film thickness [24,30]. Nevertheless, the values of refractive index are more accurate because the exact maxima or minima on transmittance curves are used [30]. It allows to calculate spectral distribution of the refractive index $n(\lambda)$ and extinction coefficient $k(\lambda)$ of the deposited material applying Swanepoel's envelope method to the optical transmission and absorption spectra experimentally recorded. The derived refractive index n = 2.50–3.25 in the visible range is very high for organic polymeric material [31,32]. These are even higher than those (2.3–2.5) for pCN fabricated by conventional "slow" CVD deposition processes [7]. The highest value belongs to the film deposited at 575 °C. Remember that this deposition temperature provides the best crystallization of the deposited material. The averaged refractive index correlates with the size of crystallites.

The deposition temperature also influences the PL spectra of the films. There are a shift of the PL intensity peak to lower energies, growth of FWHM of integral PL band and a monotonic drop of the direct energy band gap caused by the growth of the deposition temperature (Table 2). These phenomena are closely related and reflect an evolution of the electronic energy bands along with the structural and atomic composition changes described above. The observed behavior of the optical characteristics of the pCN films is a result of growing polymerization rate of the material at higher deposition temperature and buildup of π-bond conjugated system based on sp^2-hybrydization lowering the band gap [26,33]. An increase of deposition duration from 3 to 5 min at the same temperature (625 °C) results in widening of the direct band gap (2.96 → 3.00 eV). Since a thicker film was deposited with the longer process duration, it means that the melamine precursor source was not yet exhausted and the synthesis process did not stop. However, heat processing of the already synthesized film material may have led to a change in their structure associated with exfoliation, partial evaporation and disruption of the π-conjugated system, which was the cause of the observed changes in the optical characteristics [34–36].

It is noteworthy that the determined indirect band gaps are almost identical in all the samples fabricated, and the observed changes of direct band gap and PL intensity peak shift are much less prominent then usually observed for series of carbon nitride materials obtained at different temperatures [37–39]. The possible reason is the levelling effect of high oxygen concentration which remains almost constant for all pCN films obtained at different synthesis temperature which neglects the variation of nitrogen excess in the samples. Therefore, the position of the minimum of the conduction band related to absorption with indirect transitions between the bands does not change, while the distance between the minimum energy of the conduction band and the maximum of the valence band in the center of the Brillouin zone increases slightly.

The average lifetime of the photogenerated carriers in the deposited pCN films are withing the expected nanosecond range determined for similar materials by other researches [26,27,40,41]. The revealed "fast" and "slow" components are defined by a complex mechanism of luminescence. It is known that several recombination paths are exist in this polymeric material [26]. The routes with a high recombination energy involve conductance and valence bands. A lower energy process corresponds to transitions via the defect levels in the band gap. The most common are impurity levels associated with oxygen and nitrogen atoms and with nitrogen electron lone pairs. Accounting for the experimental results obtained, our samples could contain all of them. Moreover, about 2.9 at.% of oxygen and affected stoichiometry of the material tend to conclude on a large excess of interstitial nitrogen atoms in the material. Hence, "slow" PL is presumably related to recombination processes via defect levels, as excited carriers could stay longer in defect states [26]. It is also supported by expanding the role of the "slow" recombination with decreasing detection wavelength, because irradiative recombination involving defect levels has lower energy compared to direct band-to-band transitions [27,40]. The "fast" component with the shortest lifetime relates to the recombination of the charge carriers confined in the highly conjugated aromatic rings of heptazine units.

The calculated average lifetimes determined using detection wavelengths from the low photon energy region are comparable to those presented elsewhere [26,27,40]. However, the lifetime determined at 420 nm is notably shorter. It mostly corresponds to high energy band-to-band recombination processes. Its decrease could be attributed to better crystallization and structurization of the film material deposited by our rapid CVD method as compared to conventional longer in time techniques.

5. Conclusion

The developed rapid CVD of pCN allows fabrication of thin films from this material as thick as 830–1547 nm on glass and silicon substrates. It has been found that synthesis of this material in a thin film form can be realized within few minutes in the temperature range from 550 to 625 °C instead of hours at these temperatures in conventional techniques. The deposited films are smooth, non-scuttering, transparent and well-structured. They consist of multiple polycrystalline layers of pCN with crystallites oriented parallel to the substrate surface. While the material contains some oxygen and excess of nitrogen its optical properties derived by optical spectrometry, as well as by photoluminescence occur to be promising for applications in electronics and optoelectronics. The deposition temperature in the range of 550–575 °C looks to be the best for that.

CRediT authorship contribution statement

Eugene Chubenko: Writing – original draft, Methodology, Data curation. **Sergey Maximov:** Investigation, Formal analysis. **Cong Doan Bui:** Investigation, Data curation. **Victor Borisenko:** Writing – review & editing, Supervision, Conceptualization.

Declaration of competing interest

The authors declare that they have no known competing financial interests or personal relationships that could have appeared to influence the work reported in this paper.

Acknowledgements

The authors are grateful to D.V. Zhigulin for the SEM and EDX analysis and to G.P. Yablonskii for the PL measurements. The authors declare no conflicts of interests. This work was funded by the Ministry of Education of the Republic of Belarus, Project 1.4, Belarus State Research Program “Material Science, Novel Materials and Technologies”.

Data availability

Data will be made available on request.

References

[1] K.S. Novoselov, A.K. Geim, S.V. Morozov, D. Jiang, Y. Zhang, S.V. Dubonos, I. V. Grigorieva, A.A. Firsov, Electric field effect in atomically thin carbon films, Science 306 (2004) 666–669, https://doi.org/10.1126/science.1102896.
[2] H.Y. Hoh, Y. Zhang, Y.L. Zhong, Q. Bao, Harnessing the potential of graphitic carbon nitride for optoelectronic applications, Adv. Opt. Mater. 9 (2021) 2100146, https://doi.org/10.1002/adom.202100146.
[3] A. Chaves, J.G. Azadani, H. Alsalman, D.R. da Costa, R. Frisenda, A.J. Chaves, S. H. Song, Y.D. Kim, D. He, J. Zhou, A. Castellanos-Gomez, F.M. Peeters, Z. Liu, C. L. Hinkle, S.-H. Oh, P.D. Ye, S.J. Koester, Y.H. Lee, Ph Avouris, X. Wang, T. Low, Bandgap engineering of two-dimensional semiconductor materials, npj 2D Mater. Appl. 4 (2020) 29, https://doi.org/10.1038/s41699-020-00162-4.
[4] W.-J. Ong, L.-L. Tan, Y.H. Ng, S.-T. Yong, S.-P. Chai, Graphitic carbon nitride (g-C_3N_4)-based photocatalysts for artificial photosynthesis and environmental remediation: are we a step closer to achieving sustainability? Chem. Rev. 116 (2016) 7159–7329, https://doi.org/10.1021/acs.chemrev.6b00075.
[5] F.K. Kessler, Y. Zheng, D. Schwarz, C. Merschjann, W. Schnick, X. Wang, M. J. Bojdys, Functional carbon nitride materials – design strategies for electrochemical devices, Materials 2 (2017) 17030, https://doi.org/10.1038/natrevmats.2017.30.
[6] X. Wang, K. Maeda, A. Thomas, K. Takanabe, G. Xin, J.M. Carlsson, K. Domen, M. Antonietti, A metal-free polymeric photocatalyst for hydrogen production from water under visible light, Nat. Mater. 8 (2009) 76–80, https://doi.org/10.1038/nmat2317.
[7] P. Giusto, D. Cruz, T. Heil, H. Arazoe, P. Lova, T. Aida, D. Comoretto, M. Patrini, M. Antonietti, Shine bright like a diamond: new light on an old polymeric semiconductor, Adv. Mater. 2020 (2020) 1908140, https://doi.org/10.1002/adma.201908140.
[8] A. Thomas, A. Fischer, F. Goettmann, M. Antonietti, J.-O. Müller, R. Schlögl, J. M. Carlsson, Graphitic carbon nitride materials: variation of structure and morphology and their use as metal-free catalysts, J. Mater. Chem. 18 (2008) 4893–4908, https://doi.org/10.1039/B800274F.
[9] J. Zhu, P. Xiao, H. Li, S.A.C. Carabineiro, Graphitic carbon nitride: synthesis, properties, and applications in catalysis, ACS Appl. Mater. Interfaces 6 (2014) 16449–16465, https://doi.org/10.1021/am502925j.
[10] A. Wang, C. Wang, L. Fu, W. Wong-Ng, Y. Lan, Recent advances of graphitic carbon nitride-based structures and applications in catalyst, sensing, imaging, and LEDs, Nano-Micro Lett. 9 (2017) 47, https://doi.org/10.1007/s40820-017-0148-2.
[11] C. Jia, L. Yang, Y. Zhang, X. Zhang, K. Xiao, J. Xu, J. Liu, Graphitic carbon nitride films: emerging paradigm for versatile applications, ACS Appl. Mater. Interfaces 12 (2020) 53571–53591. doi: 10.1021/acsami.0c15159.
[12] P.C. Patra, Y.N. Mohapatra, Dielectric constant of thin film graphitic carbon nitride (g-C3N4) and double dielectric Al_2O_3/g-C_3N_4, Appl. Phys. Lett. 118 (2021) 103501, https://doi.org/10.1063/5.0045911.
[13] L. Chen, R. Yan, M. Oschatz, L. Jiang, M. Antonietti, K. Xiao, Ultrathin 2D graphitic carbon nitride on metal films: underpotential sodium deposition in adlayers for sodium-ion batteries, Angew. Chem., Int. Ed. 59 (2020) 9067–9073, https://doi.org/10.1002/anie.202000314.
[14] P. Giusto, B. Kumru, D. Cruz, M. Antonietti, Optical anisotropy of carbon nitride thin films and photographed polystyrene brushes, Adv. Opt. Mater. 10 (2022) 2101965, https://doi.org/10.1002/adom.202101965.
[15] P. Giusto, H. Arazoe, D. Cruz, P. Lova, T. Heil, T. Aida, M. Antonietti, Boron carbon nitride thin films: from disordered to ordered conjugated ternary materials, J. Am. Chem. Soc. 142 (2020) 20883–20891, https://doi.org/10.1021/jacs.0c10945.
[16] E.B. Chubenko, N.G. Kovalchuk, I.V. Komissarov, V.E. Borisenko, Chemical vapor deposition of 2D crystallized g-C3N4 layered films, J. Phys. Chem. C. 126 (2022) 4710–4714, https://doi.org/10.1021/acs.jpcc.1c10561.
[17] H. Arazoe, D. Miyajima, K. Akaike, F. Araoka, E. Sato, T. Hikima, M. Kawamoto, T. Aida, An autonomous actuator driven by fluctuations in ambient humidity, Nat. Mater. 15 (2016) 1084–1090, https://doi.org/10.1038/nmat4693.
[18] A. Sudhaik, P. Raizada, P. Shandilya, D.-Y. Jeong, J.-H. Lim, P. Singh, Review on fabrication of graphitic carbon nitride based efficient nanocomposites for photodegradation of aqueous phase organic pollutants, J. Ind. Eng. Chem. 67 (2018) 28–51, https://doi.org/10.1016/j.jiec.2018.07.007.
[19] E.B. Chubenko, S.E. Maximov, C.D. Bui, V.T. Pham, V.E. Borisenko, Rapid chemical vapor deposition of graphitic carbon nitride films, Materialia 28 (2023) 101724, https://doi.org/10.1016/j.mtla.2023.101724.
[20] R. Swanepoel, Determination of the thickness and optical constants of amorphous silicon, J. Phys. E Sci. Instrum. 16 (1983) 1214–1222, https://doi.org/10.1088/0022-3735/16/12/023.
[21] R. Swanepoel, Determination of surface roughness and optical constants of inhomogeneous amorphous silicon films, J. Phys. E Sci. Instrum. 17 (1984) 896–903, https://doi.org/10.1088/0022-3735/17/10/023.
[22] E.R. Shaaban, I.S. Yahia, E.G. El-Metwally, Validity of Swanepoel’s method for calculating the optical constants of thick films, Acta Phys. Pol., A 121 (2012) 628–635, https://doi.org/10.12693/APhysPolA.121.628.
[23] S. Jena, R.B. Tokas, S. Thakur, D.V. Udupa, PRISA: a user-friendly software for determining refractive index, extinction co-efficient, dispersion energy, band gap, and thickness of semiconductor and dielectric thin films, Nano Express 2 (2021) 010008, https://doi.org/10.1088/2632-959X/abd967.
[24] Y. Jin, B. Song, Z. Jia, Y. Zhang, C. Lin, X. Wang, S. Dai, Improvement of Swanepoel method for deriving the thickness and the optical properties of chalcogenide thin films, Opt. Express 25 (2017) 440–451, https://doi.org/10.1364/OE.25.000440.
[25] Y. Fang, D. Jayasuriya, D. Furniss, Z.Q. Tang, Ł. Sojka, C. Markos, S. Sujecki, A. B. Seddon, T.M. Benson, Determining the refractive index dispersion and thickness of hot-pressed chalcogenide thin films from an improved Swanepoel method, Opt. Quant. Electron. 49 (2017) 237, https://doi.org/10.1186/2251-7235-6-13.
[26] B. Choudhury, K.K. Paul, D. Sanyal, A. Hazarika, P.K. Giri, Evolution of nitrogen-related defects in graphitic carbon nitride nanosheets probed by positron annihilation and photoluminescence spectroscopy, J. Phys. Chem. C 122 (2018) 9209–9219, https://doi.org/10.1021/acs.jpcc.8b01388.
[27] Y. Zhang, Q. Pan, G. Chai, M. Liang, G. Dong, Q. Zhang, J. Qiu, Synthesis and luminescence mechanism of multicolor-emitting g-C_3N_4 nanopowders by low temperature thermal condensation of melamine, Sci. Rep. 3 (2013) 1943, https://doi.org/10.1038/srep01943.
[28] F. Fina, S.K. Callear, G.M. Carins, J.T.S. Irvine, Structural investigation of graphitic carbon nitride via XRD and neutron diffraction, Chem. Mater. 27 (2015) 2612–2618, https://doi.org/10.1021/acs.chemmater.5b00411.
[29] B. Jürgens, E. Irran, J. Senker, P. Kroll, H. Müller, W. Schnick, Melem (2,5,8-triamino-tri-s-triazine), an important intermediate during condensation of melamine rings to graphitic carbon nitride: synthesis, structure determination by X-ray powder diffractometry, solid-state NMR, and theoretical studies, J. Am. Chem. Soc. 125 (2003) 10288–10300, https://doi.org/10.1021/ja0357689.
[30] D. Dorranian, L. Dejam, G. Mosayebian, Optical characterization of Cu_3N thin film with Swanepoel method, J. Theor. Appl. Phys. 6 (2012) 13,. doi:10.1186/2251-7235-6-13.
[31] T. Higashihara, M. Ueda, Recent progress in high refractive index polymers, Macromolecules 48 (2015) 1915–1929, https://doi.org/10.1021/ma502569r.
[32] M. Campoy-Quiles, M.I. Alonso, D.D.C. Bradley, L.J. Richter, Advanced ellipsometric characterization of conjugated polymer films, Adv. Funct. Mater. 24 (2014) 2116–2134, https://doi.org/10.1002/adfm.201303060.
[33] Y. Jiang, Z. Sun, C. Tang, Y. Zhou, L. Zeng, Enhancement of photocatalytic hydrogen evolution activity of porous oxygen doped g-C_3N_4 with nitrogen defects induced by changing electron transition, Appl. Catal., B 240 (2019) 30–38, https://doi.org/10.1016/j.apcatb.2018.08.059.

[34] F. Dong, Y. Li, Z. Wang, W.K. Ho, Enhanced visible light photocatalytic activity and oxidation ability of porous graphene-like g-C_3N_4 nanosheets via thermal exfoliation, Appl. Surf. Sci. 358 (2015) 393–403, https://doi.org/10.1016/j.apsusc.2015.04.034.

[35] J. Fu, B. Zhu, C. Jiang, B. Cheng, W. You, J. Yu, Hierarchical porous O-doped g-C_3N_4 with enhanced photocatalytic CO_2 reduction activity, Small 13 (2017) 1603938, https://doi.org/10.1002/smll.201603938.

[36] Z. Zhao, Y. Sun, Q. Luo, F. Dong, H. Li, W.K. Ho, Mass-controlled direct synthesis of graphene-like carbon nitride nanosheets with exceptional high visible light activity. Less is better, Sci. Rep. 5 (2015) 14643, https://doi.org/10.1038/srep14643.

[37] G. Zhang, J. Zhang, M. Zhang, X. Wang, Polycondensation of thiourea into carbon nitride semiconductors as visible light photocatalysts, J. Mater. Chem. 22 (2012) 8083–8091, https://doi.org/10.1039/c2jm00097k.

[38] Y. Yuan, L. Zhang, J. Xing, M.I.B. Utama, X. Lu, K. Du, Y. Li, X. Hu, S. Wang, A. Genç, R. Dunin-Borkowski, J. Arbiold, Q. Xiong, High-yield synthesis and optical properties of g-C_3N_4, Nanoscale 7 (2015) 12343–12350, https://doi.org/10.1039/c5nr02905h.

[39] D. Das, D. Banerjee, D. Pahari, U.K. Ghorai, S. Sarkar, N.S. Das, K. K. Chattopadhyay, Defect induced tuning of photoluminescence property in graphitic carbon nitride nanosheets through synthesis conditions, J. Lumin. 185 (2017) 155–165, https://doi.org/10.1016/j.jlumin.2017.01.007.

[40] Z. Gan, Y. Shan, J. Chen, Q. Gui, Q. Zhang, S. Nie, X. Wu, The origins of the broadband photoluminescence from carbon nitrides and applications to white light emitting, Nano Res. 9 (2016) 1801–1812, https://doi.org/10.1007/s12274-016-1073-2.

[41] C. Merschjann, T. Tyborski, S. Orthmann, F. Yang, K. Schwarzburg, M. Lublow, M.-Ch Lux-Steiner, Th Schedel-Niedrig, Photophysics of polymeric carbon nitride: an optical quasimonomer, Phys. Rev. B 87 (2013) 205204, https://doi.org/10.1103/PhysRevB.87.205204.